

Electronic Supporting Information

Halogen-Assisted Colour Modulation in Flexible Copper Coordination Polymer Crystals Based Hybrid Photonic Splitter

Ankur Khapre, Vinaya Durga Chebrolu, Preetika Rajasekar, Biswajit Kumar Barman, Rajadurai Chandrasekar

School of Chemistry and Centre for Nanotechnology, University of Hyderabad, Prof. C. R. Rao Road, Gachibowli, Hyderabad 500 046, Telangana, India.

E-mail: r.chandrasekar@uohyd.ac.in

Table of Contents:

Serial No.	Title	Page No.
1	Materials	S3
2	Instrumental Methods	S3-4
3	Synthesis and Crystallization a) Synthesis for CuBCP and CuDBP molecules. (Scheme S1) b) Solvent-based growth of crystals. (Figure S1-S2)	S5-6
4	FT-IR of CuBCP and CuDBP (Figure S3)	S7
5	PXRD of CuBCP and CuDBP (Figure S4)	S7
6	X-ray Diffraction studies of CuBCP and CuDBP a) Single crystal X-ray unit cell parameter data. (Table S1) b) SAED pattern plane indexing and comparison with SCXRD data. (Figure S5)	S8
7	Qualitative mechanical properties Nanoindentation data. (Figure S6)	S9
8	Theoretical calculations of CuBCP and CuDBP Spatial plots of frontier molecular orbital energies of HOMO and LUMO for CuBCP and CuDBP. (Figure S7)	S9-10
9	Solid-state (FLIM) optical lifetime studies of CuBCP and CuDBP FL lifetime decay of CuBCP and CuDBP. (Figure S8)	S10
10	Formulas and Equations a) Photoluminescence Quantum Yield (PLQY) calculation (Eq. S1) b) Strain calculations (Equation S2) c) Optical loss calculations (Equation S3) d) Nanoindentation calculations	S11

	<p>i) Hardness calculation (Equations S4 and S5)</p> <p>ii) Young's modulus calculation (Equation S6)</p>	
11	<p>Optical waveguiding studies</p> <p>a) Optical waveguiding of CuDBP crystal. (Figure S9)</p> <p>b) Optical waveguiding of CuBCP crystal. (Figure S10)</p> <p>c) Position-dependent and optical waveguiding in CuBCP straight and bent crystals. (Figure S11)</p>	S12-13
12	<p>1×2 Y-splitter fabrication and its optical waveguiding studies</p> <p>a) Transferring CuBCP crystal from substrate-1 to substrate-2. (Figure S12)</p> <p>b) Optical waveguiding of CuBCP crystal. (Figure S13)</p> <p>c) Crystal cutting by micromanipulation technique. (Figure S14)</p> <p>d) Crystal bending images of CuBCP. (Figure S15)</p> <p>Micromanipulation of CuDBP and fabrication of Y-splitter. (Figure S16-S17)</p>	S14-16
13	References	S17

1. Materials

Copper(I) iodide and potassium iodide were purchased from Finar Chemicals Ltd. 3-Bromo-5-Chloropyridine and 3,5-Dibromopyridine were purchased from BLD pharma. HPLC grade acetone and acetonitrile were obtained from Merck Ltd. The chemicals and solvents were used as received unless specified. Millipore water was used for the studies unless otherwise stated. Borosilicate coverslips (Borosil) of thickness ≈ 0.1 mm were obtained from Bluestar glass suppliers. Square pattern of 200 mesh copper TEM grids was purchased from commercial suppliers.

2. Instrumental Methods

a) FT-IR Spectroscopy studies

The FT-IR spectra were recorded using an iD7-ATR detector attached to the Thermo Scientific iS5 instrument.

b) Absorbance and emission studies

The UV-visible absorption measurements were done using a JASCO V-750 spectrometer in a diffuse reflectance UV-visible (DR-UV-vis) mode. The reflectance spectra were converted to an absorbance one using the Kubelka-Munk function. The solid-state emission spectra and photoluminescence quantum yield were collected using a JASCO FP-8500 spectrofluorometer.

c) Single crystal X-ray diffraction studies

Single crystal X-ray diffraction (SCXRD): SCXRD data was collected for the microcrystal on a Rigaku (dual, Cu/Mo at zero Eos) diffractometer using monochromatic Cu- K_{α} radiation having a 100 μm beam size. The structure was solved by Olex2 (1.2.9 version) with the SHELXT structure solution program via intrinsic phasing algorithm and the ShelXL refinement package using Least Squares minimization was utilized to refine the structure. 1-2 Displacement parameters of all non-hydrogen atoms were refined anisotropically. Mercury (4.2.0 version) software was used to prepare all the crystal packing diagrams.

d) Nanoindentation studies

Nanoindentation experiments were conducted on a flat, highly smooth crystal surface using an Oxford Asylum AFM microscope. Indentations were performed in indentation mode with a four-side-cone-shaped synthetic diamond tip (ADAMA INNOVATIONS NM-TC) featuring a half-angle of 45°. The spring constant (k) of the AFM cantilever was calculated using the relation $k = A Q f^{1.3}$, where the coefficient $A = 8.296 \times 10^{-9}$ was provided by the tip manufacturer.

The quality factor ($Q \approx 1000$) and resonance frequency ($f \approx 775$ kHz) were obtained through the system's auto-tuning function. The Inverse Optical Lever Sensitivity (InvOLS, 130 nm/V) was determined using the Sader method.¹ For this, indentations were performed on a hard sapphire substrate, and InvOLS was extracted by fitting the slope of the deflection (V) vs. displacement (nm) curve. To calibrate mechanical property measurements, borosilicate glass was used as a standard reference sample, with reported Young's modulus and hardness values of 79 GPa and 5.7 GPa, respectively. The Young's modulus of the crystal was determined using the Oliver–Pharr method implemented in Asylum Research software (v16.25.226), while hardness values were calculated based on equations S4 and S5.²

e) Confocal optical microspectroscopy studies

The optical experiments of a single microcrystal were carried out on a backscattering mode setup of the Wi-Tec alpha 300 AR laser confocal optical microscope (LCOM) equipped with a Peltier-cooled CCD detector. Using 300 grooves/mm grating BLZ = 750 nm, the accumulation time was adjusted to 30 s and the integration time was typically made 0.5 s. Ten averaged accumulations are obtained for every single spectrum. A diode 405 nm laser source was used for optical excitation of the polymorphic crystal waveguides via a 60× objective. Unless otherwise specified, 20× objectives were used for spectra and image collection. All the experiments were carried out under ambient conditions.

f) Mechanical micromanipulation of crystals

Micromanipulation was performed on the CP crystals using the front AFM tips attached to the inertial drive of the confocal microscope mentioned above. The manipulation is usually performed on the crystal-containing substrate using the three-dimensional movement of the stage while the AFM tips are kept constant.

g) Field-Emission scanning electron microscopy studies

The circuit morphology was analyzed by using a Zeiss field-emission scanning electron microscope (FE-SEM) operating at 5 kV. All the experiments were performed after ≈ 10 nm gold coating the samples before imaging.

h) Fluorescence lifetime imaging microscopy studies

FL lifetime decay plots were recorded using a time-resolved confocal fluorescence lifetime imaging instrument (Pico Quant, Micro-Time 200), which was equipped with an inverted Olympus IX 71 microscope. The crystals were dispersed on a coverslip and excited with a

solid-state 405 nm picosecond pulse laser with a power output of 5 μ W, with a fixed repetition rate of 20 MHz (FWHM: 176 ps). The signal was collected using the water-immersible Olympus UPlans (Apo; 60x; NA 1.2) objective, and filtered out the laser beam using a 430 nm long pass filter. The signal acquisition was done by using a PicoHarp 300 time-correlated single-photon counting module. The analysis of the collected signal was carried out using SymPhoTime software. All the measurements were performed at RT.

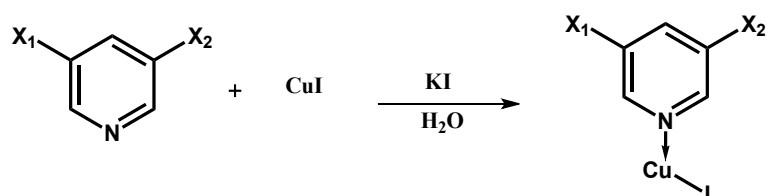
3. Synthesis of CuBCP and CuDBP

In a 250 mL conical flask, add 25 mL of Millipore water and then add excess CuI (0.400 g; 2.1 mmol) and add 1-2 spatulas of KI into the solution, which serves as the bottom layer, and sonicate it for 5 minutes. Then, slowly add acetonitrile (25 mL) from the walls of the conical flask as the middle layer, which acts as a buffer. To this, the ligand 3-Bromo-5-Chloropyridine (BCP, 0.404 g; 2.1 mmol) dissolved in acetone (10 mL) was added as a top layer and kept undisturbed. After one day, fine green emissive single crystals of CuBCP were observed at the bottom of the conical flask. Fine crystals of CuBCP were successfully obtained by separating them with the help of a spatula and kept on the cotton to absorb excess water. For CuDBP, the same procedure was followed to get cyan emissive single crystals, respectively.

Here more detailed crystal synthesis procedure:

- **Crystallisation vessel:** The 250 mL conical flask was taken for the three-layer crystallization process.
- **Bottom layer:** Saturated aqueous solution of CuI and KI (400 mg CuI + \approx 850mg KI (saturated KI solution) in 5 mL H₂O) and dilution up to 25 mL. The white is appearing due to sparing solubility of CuI in water, while excess iodide of KI allows it to form [CuI₂]⁻ complexes, which is a transparent and homogeneously saturated solution.
- **Middle buffer layer:** 8–10 mL of acetonitrile was gently added along the conical flask vessel wall on top of the bottom layer. The role of the buffer layer is to prevent the immediate mixing of the two ligand solutions (top layer) with the [CuI₂]⁻ complexes solutions (bottom layer). The major advantage of this layer is the slow approach of ligand molecules towards [CuI₂]⁻ complexes solutions, and the resulting coordination polymer crystal will be more likely to be flexible.
- **Top layer:** 10 mL of ligand solution in acetone (2.1 M solution of 3-bromo-5-chloropyridine (BCP) or 3,5-dibromopyridine (DBP)) was slowly added to the conical flask without disturbing the bottom layer.

- **Temperature:** Ambient (25 ± 5 °C)
- **Duration:** 24 hours undisturbed
- **Layer thicknesses:** Approximately 1.5 cm (aqueous), 0.5 cm (acetonitrile), 1 cm (acetone with ligand)



For CuBCP $\text{X}_1 = \text{Cl}$, $\text{X}_2 = \text{Br}$ CuDBP $\text{X}_1 = \text{Br}$, $\text{X}_2 = \text{Br}$

Scheme S1. Synthesis of CuBCP and CuDBP coordination polymer complexes.

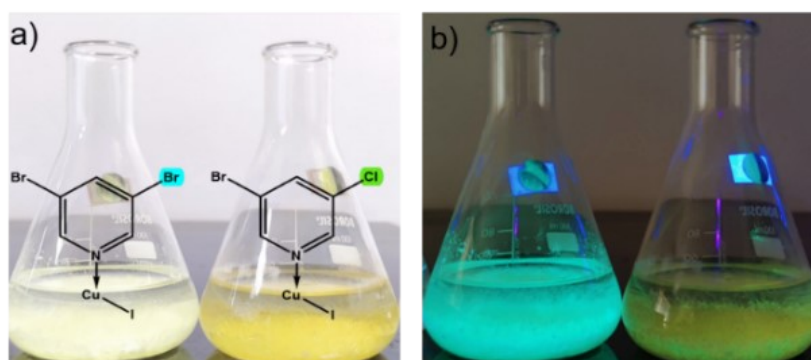


Figure S1. Photographs of conical flasks containing CuDBP and CuBCP from left to right in a) ambient and b) UV light, respectively.

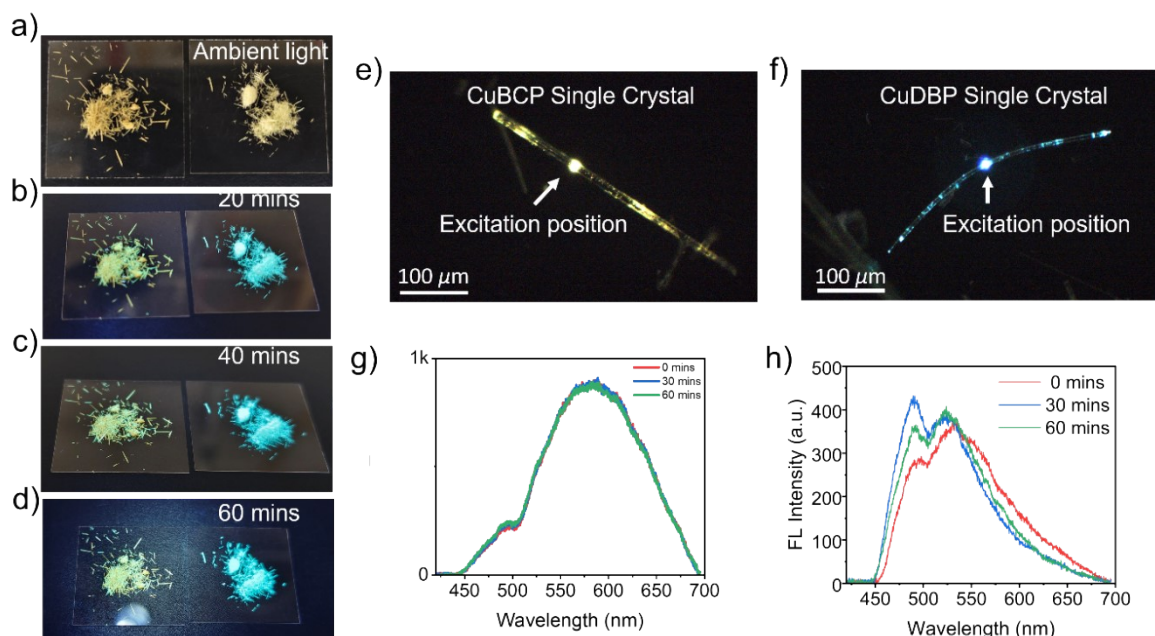


Figure S2. a-d) Photographs showing prolonged exposure of microcrystals under 365 nm (UV) light. e,f) Waveguide stability test of CuBCP and CuDBP single crystals, respectively, and g,h) confocal optical plots of corresponding crystals for different time intervals.

4. FT-IR spectroscopy of CuBCP and CuDBP

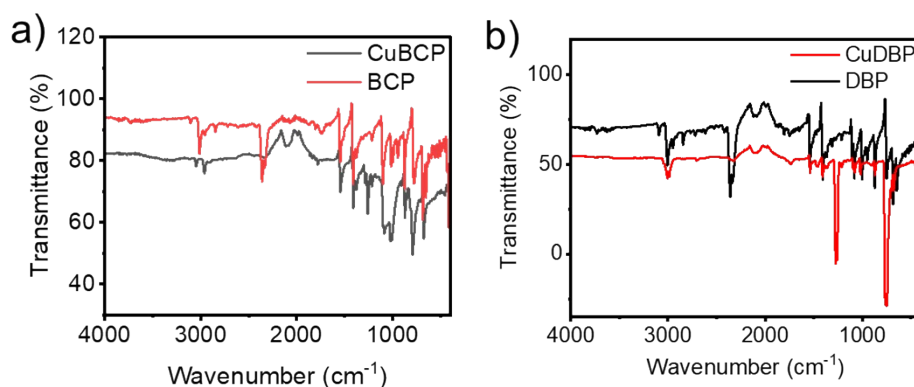


Figure S3. FT-IR data comparison with a) BCP ligand with CuBCP crystals, and b) DBP ligand with CuDBP crystals, respectively.

5. Powder X-ray Diffraction studies of CuBCP and CuDBP

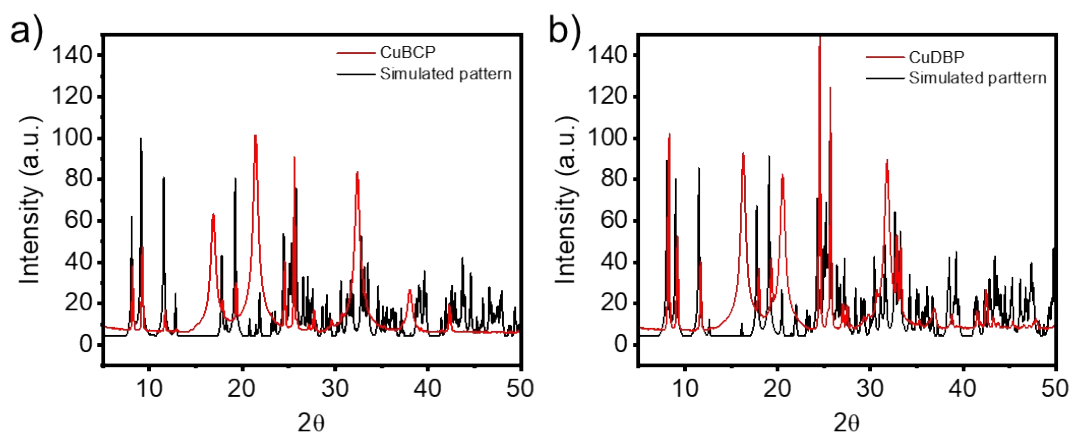


Figure S4. Comparison of experimental PXR data of a) CuBCP and b) CuDBP crystals with the simulated PXR (obtained from single-crystal) data.

6. X-ray Diffraction studies of CuBCP and CuDBP

a. Single-crystal X-ray unit cell parameter data

Table S1. Single-crystal X-ray unit cell parameter data for CuBCP and CuDBP.

Name	CuBCP	CuDBP
Molecular name	Poly-[di- μ -iodido-bis[3-bromo-5-chloropyridine] dicopper(I)]	Poly-[di- μ -iodido-bis[3,5-dibromopyridine] dicopper(I)]
CCDC	2434224	2432154
Molecular formula	C ₅ H ₃ Br Cl Cu I N	C ₅ H ₃ Br ₂ Cu I N
Crystal system	Monoclinic	Monoclinic
Space group	C2/c	C2/c
Cell length (Å)	a =21.9464, b =4.2129, c =19.5034	a =22.069, b =4.2178, c =19.750
Cell angles (°)	α =90, β =95.950, γ =90	α =90, β =95.324, γ =90
Cell volume (Å ³)	1793.53	966.413
z	8	8

b. SAED pattern plane indexing and comparison with SCXRD data

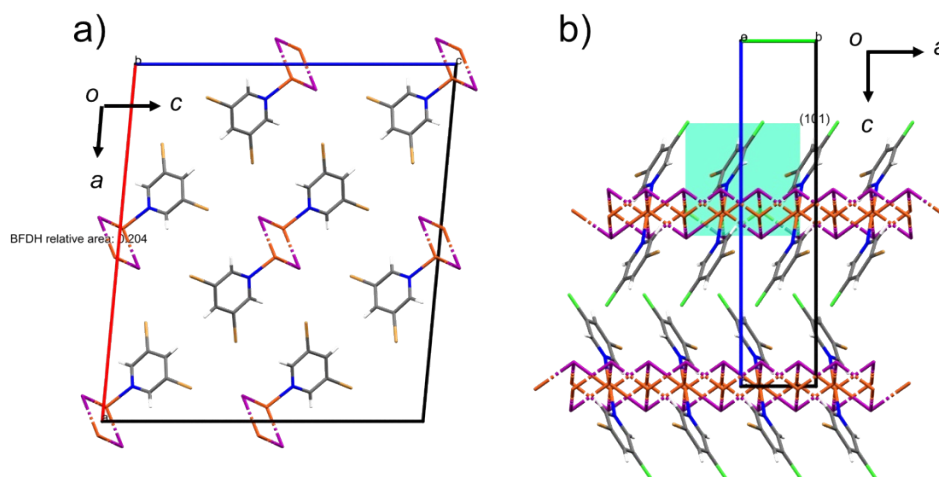


Figure S5. a) The (200) planes of the CuDBP single crystal are aligned along the b-axis, corresponding to a *d*-spacing of 0.36 nm observed in the SAED pattern. b) The (101) plane of the CuBCP single crystal matches with a *d*-spacing of 0.34 nm in the SAED pattern.

7. Nanoindentation data from AFM.

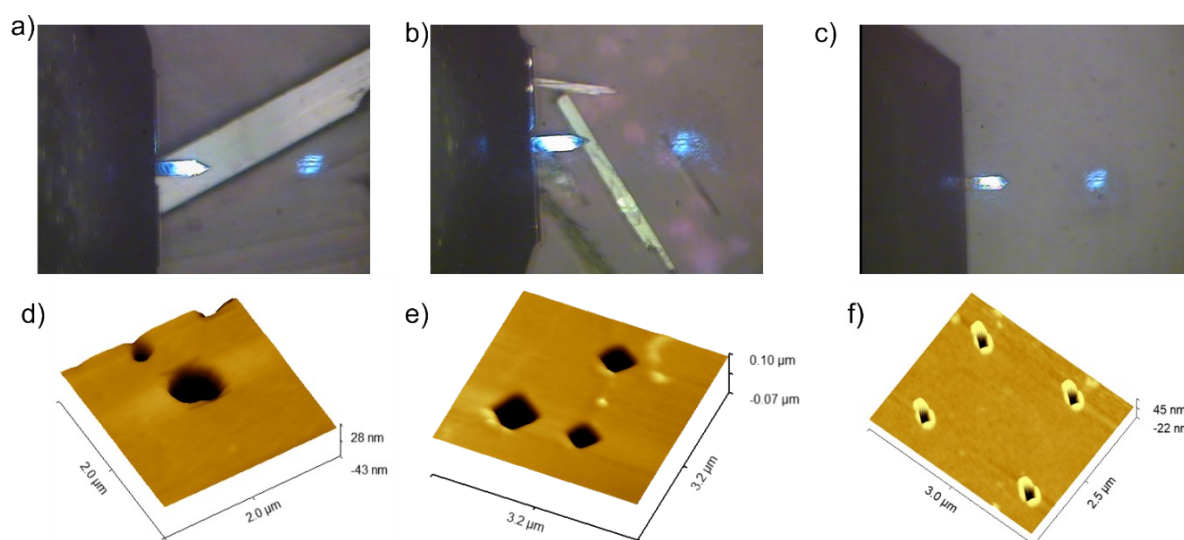


Figure S6. a,b) Optical images of approaching the AFM tip towards the CuBCP and CuDBP crystals for nanoindentation, respectively, and the associated d,e) AFM tapping mode topography images of the indented area. c,f) An optical image of the borosilicate glass during the indentation using an AFM tip and its topography image after the indentation was performed.

8. Theoretical calculations of CuBCP and CuDBP

Density functional theory (DFT) and time-dependent DFT (TD-DFT) simulations were carried out to examine the frontier molecular orbitals distribution, electrostatic potential (ESP) mapping, and excited-state characteristics of CuBCP and CuDBP. All computations were executed using the Gaussian16 software package,³ employing Becke's three-parameter functional in tandem with the correlation functional proposed by Lee, Yang, and Parr (B3LYP), which is a hybrid exchange correlation method, along with the LANL2DZ basis set. The frontier molecular orbitals (FMOs) and ESP mapping were displayed using GaussView 6.0 software.⁴ The isovalue used for FMOs was 0.03. The ESP maps used surface potential ranges [-0.02 au (red) to 0.02 au (blue)] and an isovalue of 0.0004 au.

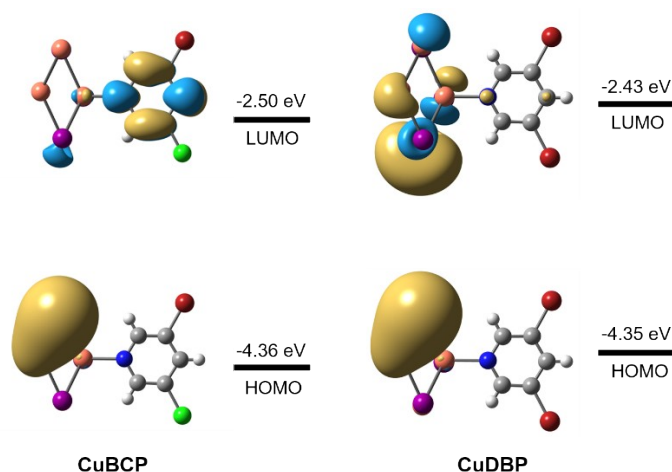


Figure S7. Spatial plot of frontier molecular orbitals (HOMO and LUMO) for CuBCP and CuDBP.

9. Solid-state (using FLIM set-up) optical lifetime studies of CuBCP and CuDBP

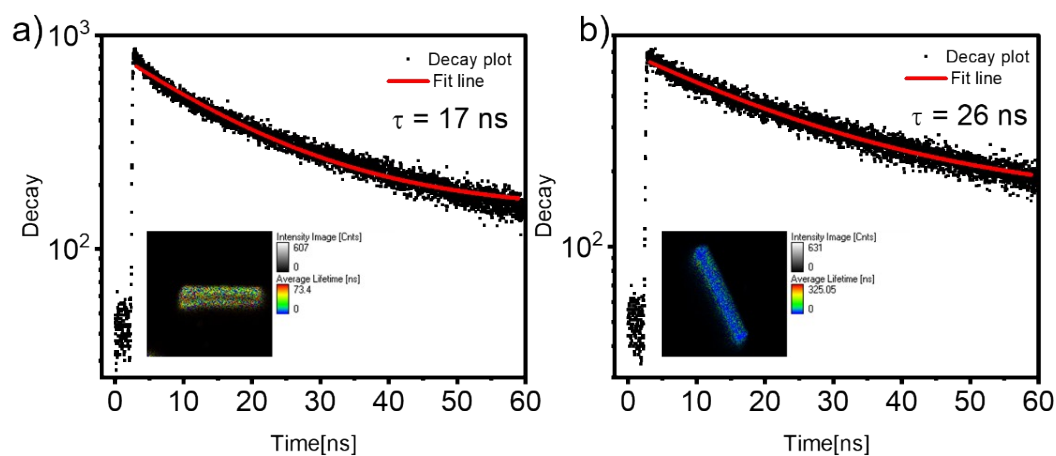


Figure S8. The fluorescence decay profiles of a) CuBCP crystals and b) CuDBP crystals were obtained by the FLIM setup. The measured photon counts were shown in red for both (CuBCP) and (CuDBP) squares on a logarithmic scale. The decays were fitted with a first-exponential fit (solid line). The inset photo represents the fluorescence lifetime images of respective crystals with an intensity image scale bar and average lifetime scale bar squares on a logarithmic scale.

10. Formulas and Equations

a. Photoluminescence Quantum Yield (PLQY) calculation:

The absolute PLQY was calculated using this formula.

$$\phi = \frac{S_2}{S_0 - S_1} \times 100\% \quad (\text{Eq. 1})$$

Where the ϕ is absolute PLQY, S_0 , S_1 , and S_2 are the areas of the incident light, scattered light from the sample, and emission from the sample, respectively.

b. Strain calculations:

The mechanical strains (ε) of the mechanically bent crystals have been calculated using the equation.

$$\varepsilon = \frac{T}{2r} \times 100\% \quad (\text{Eq. 2})$$

where r is the radius of the hypothetical radius of curvature of the bent region, and T is the crystal thickness in the strain pseudoplastic area of the crystal.

c. Optical loss calculations:

The optical loss (α) in nepers of the crystals has been calculated using the equation.

$$\frac{I_{tip}}{I_{body}} = e^{-\alpha L} \quad (\text{Eq. 3})$$

Where the I_{tip} and I_{body} are the signal intensities at the collection and excitation position separated by the length (L) of the waveguides. [α' (dB mm⁻¹) = α (mm⁻¹) × 4.343]

d. Nanoindentation calculations:

i. Hardness calculation

$$H = \frac{F}{A} \quad (\text{Eq. 4})$$

Where the H is a hardness, F is applied force in μN , and A is the area of the indent site.

$$A = \pi h^2 \tan^2(\theta) \quad (\text{Eq. 5})$$

Where h is the depth of the indent, and θ is the half angle of the cone-shaped diamond tip.

ii. Young modulus calculation using Oliver-Pharr model

$$\frac{1}{E} = \frac{1 - \nu^2}{\left(\frac{1}{E_r} - \frac{1 - \nu_i^2}{E_i} \right)} \quad (\text{Eq. 6})$$

Where E and ν are the Young's Modulus and Poisson's ratio of the material, E_i and ν_i are Young's modulus and Poisson's ratio of the indenter tip. E_r reduced modulus.

$$E_r = \frac{1\sqrt{\pi} S}{2 \beta \sqrt{A_c}} \quad (\text{Eq. 7})$$

Young's modulus, where S is stiffness dP/dh, β is correction factor, A_c = contact area.

11. Optical waveguiding studies

a. CuDBP crystal

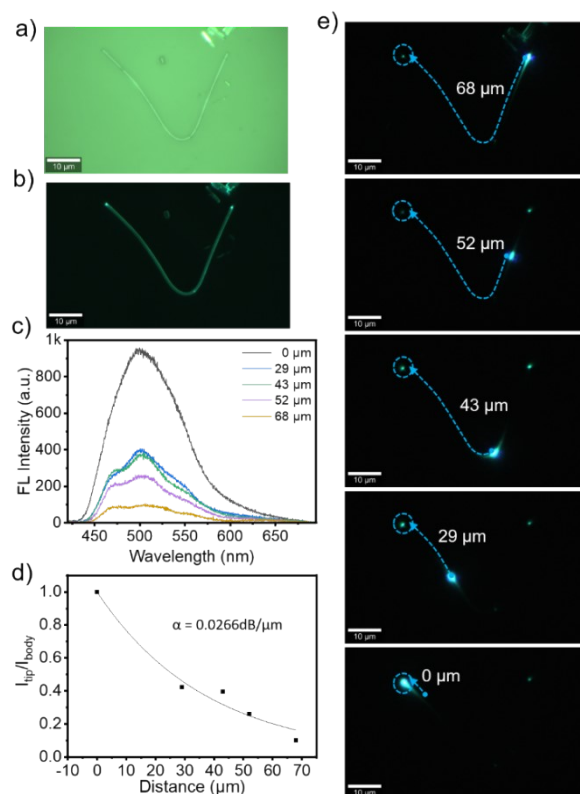


Figure S9. a) Confocal optical and b) FL microscope images of CuDBP crystal. c) FL spectra collected for a naturally grown CuDBP crystal and its corresponding d) optical loss calculation. e) FL images of the CuDBP crystal for various excitation points with a 405 nm CW laser.

b. CuBCP crystal

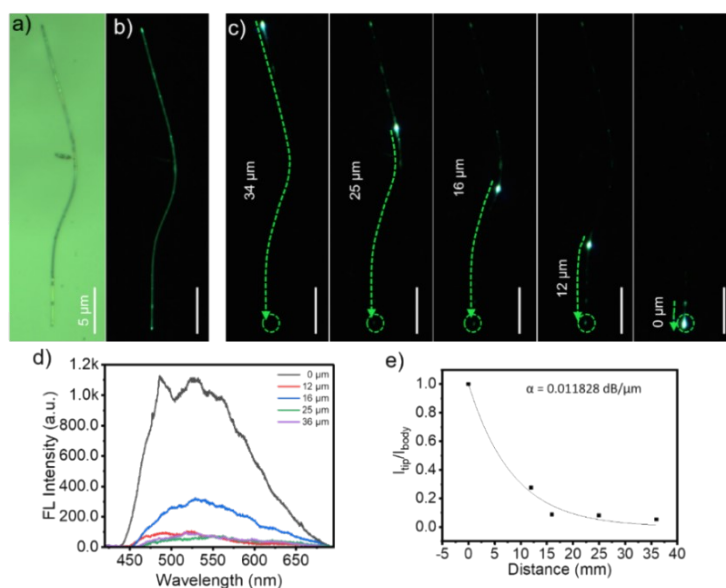


Figure S10. a) Confocal optical and b) FL microscope images of CuBCP crystal. c) Position-dependent FL images, d) FL spectra collected for CuBCP crystal and its corresponding e) Optical loss plot.

c. Position-dependent and optical waveguiding in CuBCP straight and bent crystals

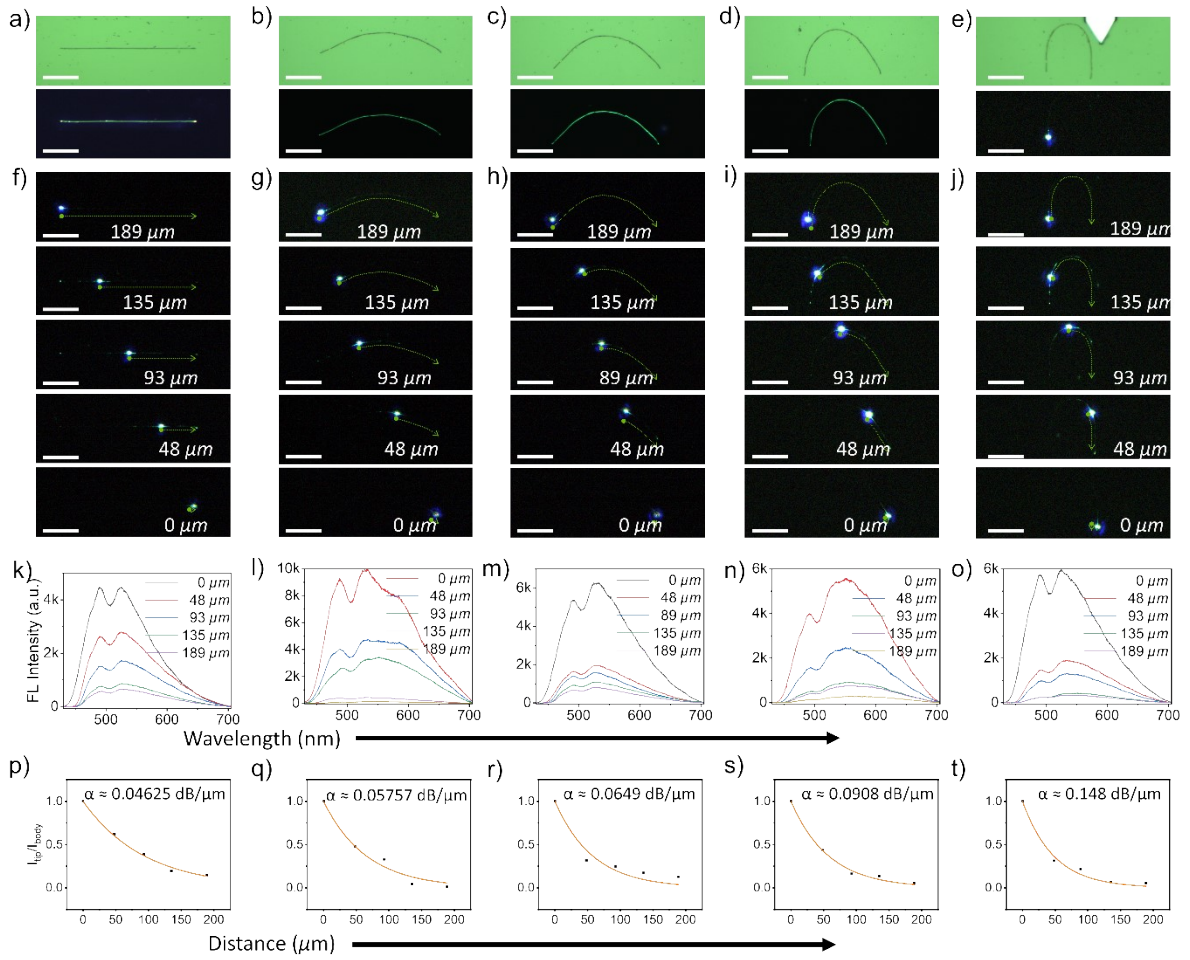


Figure S11. a-e) Sequential confocal optical and FL microscope images of mechanically bending a CuBCP crystal with an AFM cantilever tip, and the associated f-j) FL images for position-dependent waveguiding experiments for the calculation of optical loss. Scale bar: $50 \mu\text{m}$. k-o) The corresponding FL spectra for the respective crystal geometries, and p-t) their optical loss plots.

12. 1×2 Y-splitter fabrication and its optical waveguiding studies

a. Transferring CuBCP crystal from substrate-1 to substrate-2

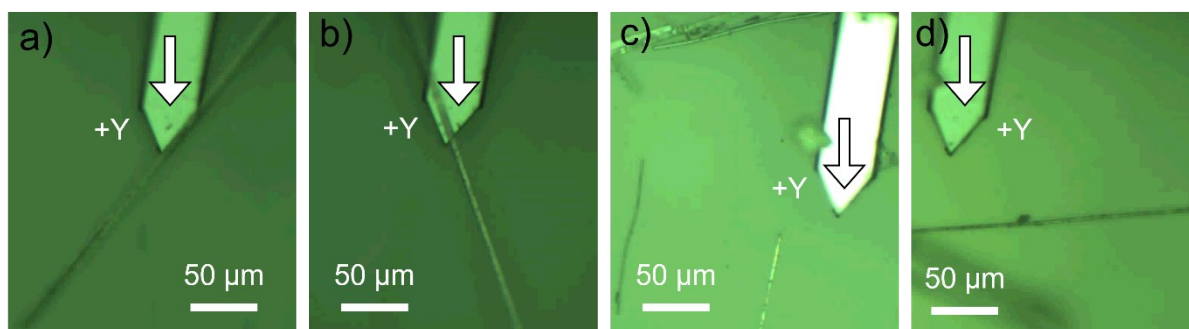


Figure S12. Optical images of a) the AFM cantilever tip approaching to the crystal on substrate-1, b) lifting from substrate-1, and c-d) transferring a long rod of CuBCP crystal to substrate-2.

b. Optical waveguiding of CuBCP crystal

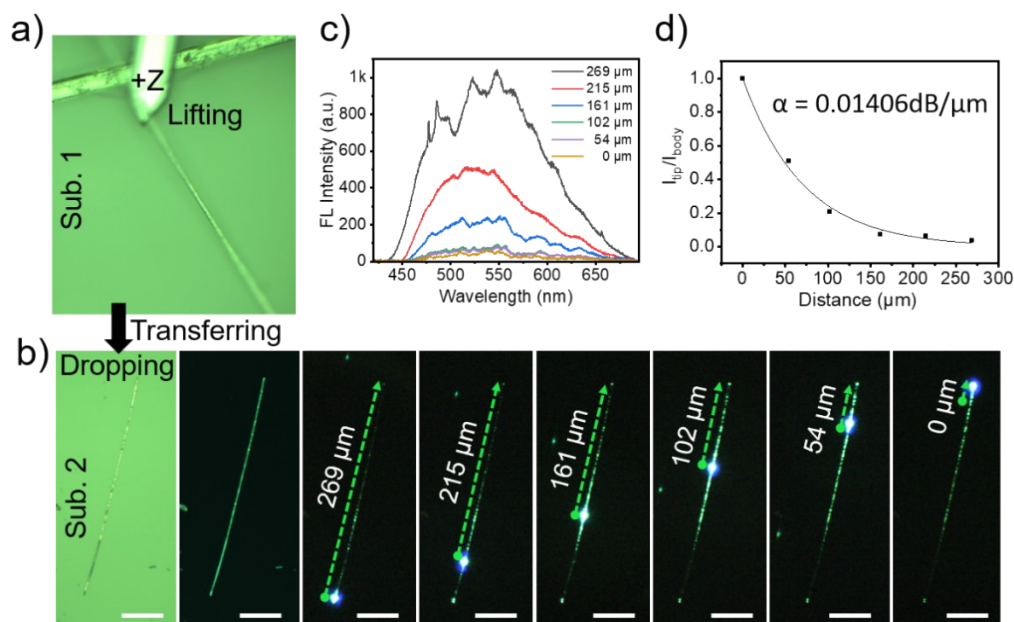


Figure S13. Confocal optical images showing a) lifting of CuBCP crystal from substrate 1, and b) dropping on substrate 2 using an AFM cantilever tip. c) FL spectra recorded for the straight crystal, and d) the optical loss plot.

c. Crystal cutting by micromanipulation technique

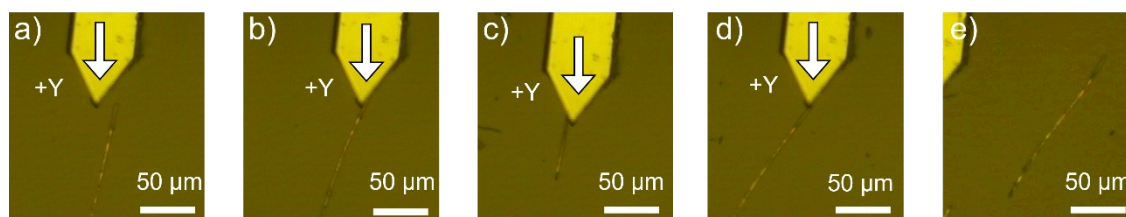


Figure S14. a-e) The AFM cantilever tip used to cut the straight CuBCP crystal.

d. Crystal bending images of CuBCP

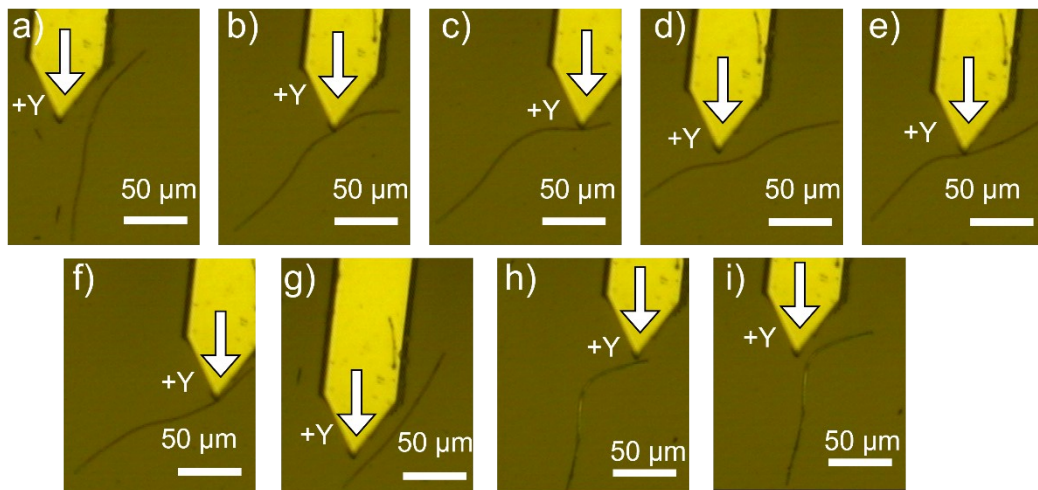


Figure S15. Confocal images of a) straight crystal of CuBCP. b) AFM cantilever tip approaching the crystal to bend it mechanically. c-e) after mechanically bending the CuBCP crystal. f-i) shows the bent form of the CuBCP crystal.

e. Micromanipulation of CuDBP and fabrication of Y-splitter

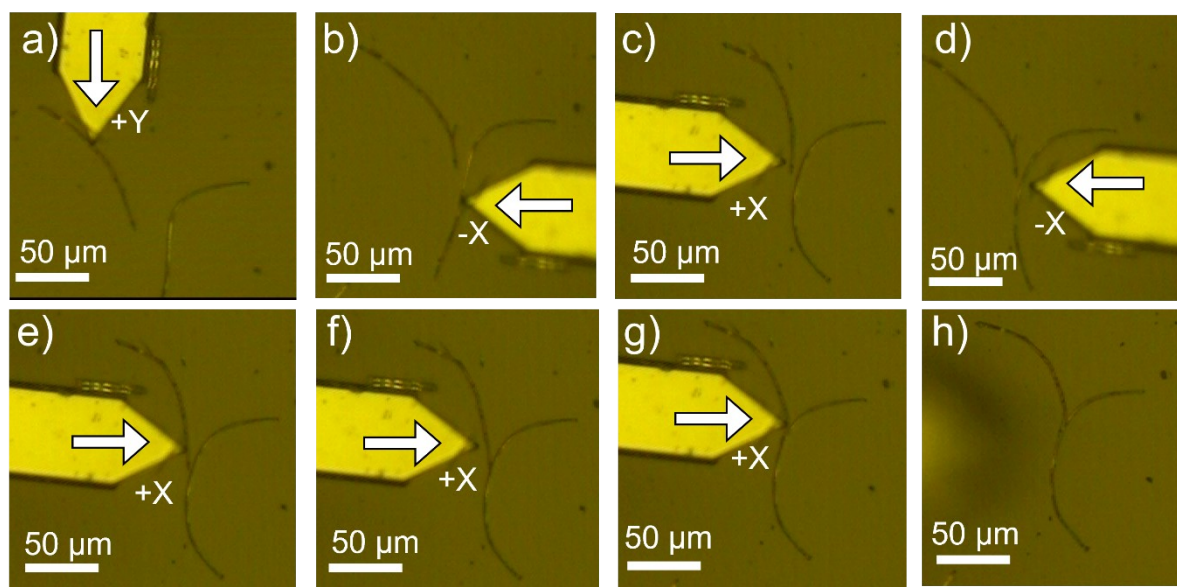


Figure S16. Confocal images of a-h) various steps are involved in the mechanical integration of bent CuBCP with the CuDBP crystal to fabricate the Y-splitter.

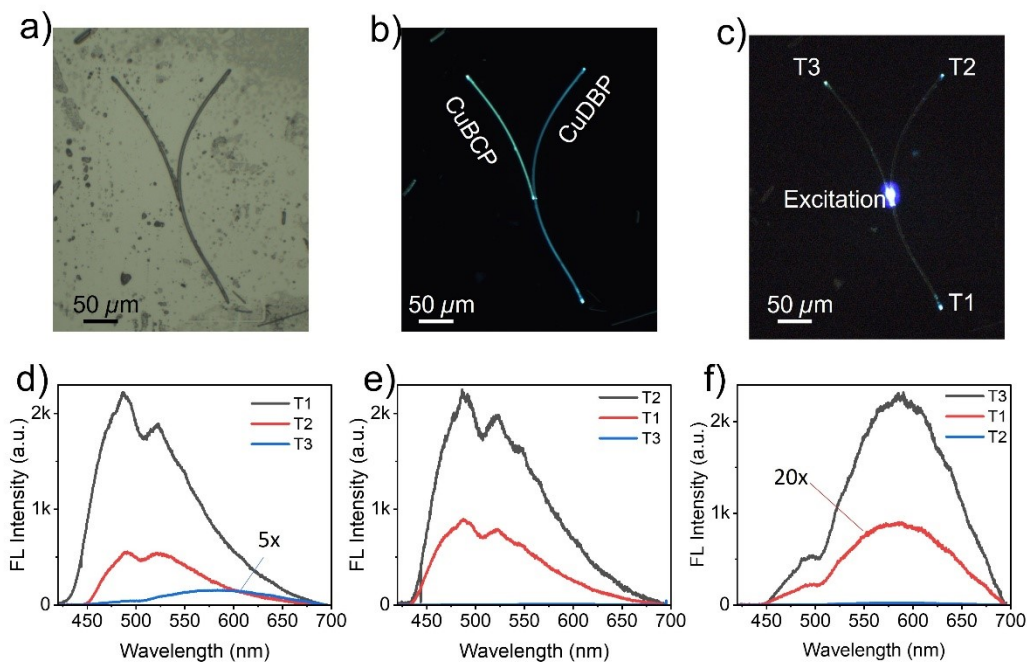


Figure S17. Refabricated hybrid optical splitter. a,b) Confocal and FL images of Y-splitter. c) FL image of optical waveguiding studies with the excitation at the junction and collection at all ports of the Y-splitter. d-f) Optical waveguiding spectra at various outputs for input at T1, T2, and T3 ports, respectively, in the Y-splitter.

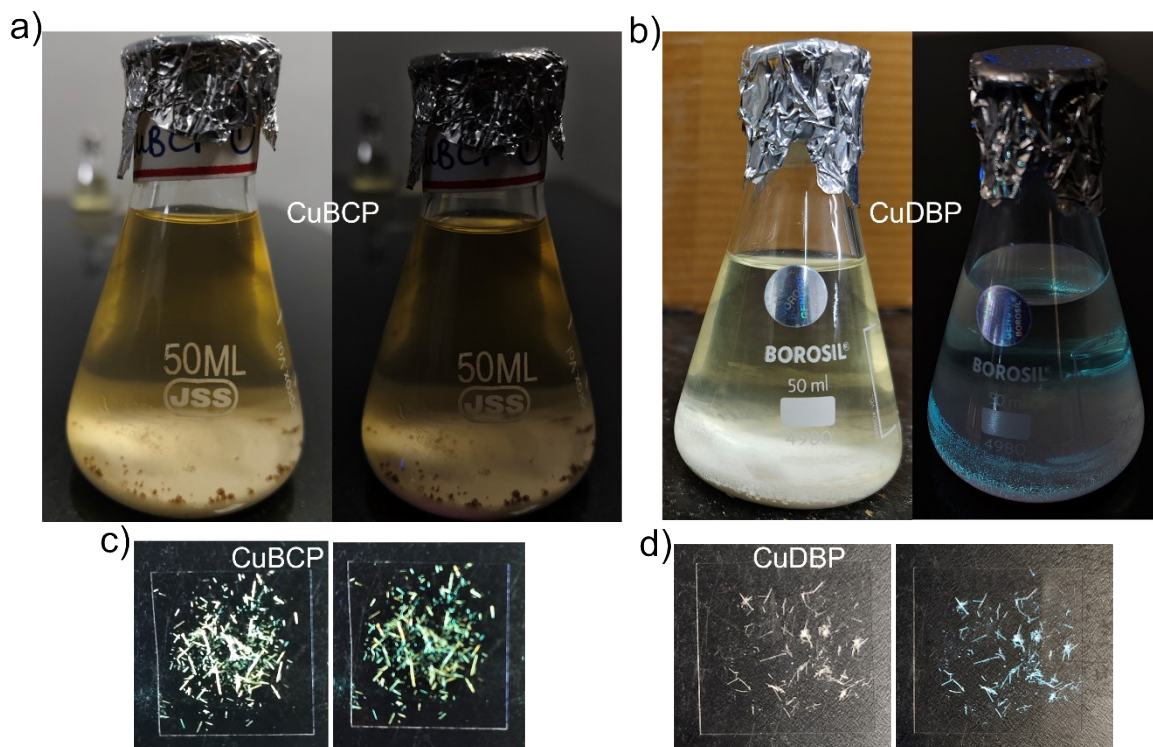


Figure S18. a,b) Test for CuBCP and CuDBP in a 1:1 ratio of acetonitrile: ethanol mixture. c,d) Insets show the corresponding single crystals.

13. References

1. J. E. Sader, J. A. Sanelli, B. D. Adamson, J. P. Monty, X. Wei, S. A. Crawford, J. R. Friend, I. Marusic, P. Mulvaney, E. J. Bieske, *Rev. Sci. Instrum.* 2012, **83**, 103705.
2. W. C. Oliver, G. M. Pharr, *J. Mater. Res.* 2004, **19**, 3-20.
3. M. J. Frisch, G. W. Trucks, H. B. Schlegel, G. E. Scuseria, M. A. Robb, J. R. Cheeseman, G. Scalmani, V. Barone, G. A. Petersson, H. Nakatsuji, X. Li, M. Caricato, A. V. Marenich, J. Bloino, B. G. Janesko, R. Gomperts, B. Mennucci, H. P. Hratchian, J. V. Ortiz, A. F. Izmaylov, J. L. Sonnenberg, D. Williams-Young, F. Ding, F. Lipparini, F. Egidi, J. Goings, B. Peng, A. Petrone, T. Henderson, D. Ranasinghe, V. G. Zakrzewski, J. Gao, N. Rega, G. Zheng, W. Liang, M. Hada, M. Ehara, K. Toyota, R. Fukuda, J. Hasegawa, M. Ishida, T. Nakajima, Y. Honda, O. Kitao, H. Nakai, T. Vreven, K. Throssell, J. A. Montgomery Jr., J. E. Peralta, F. Ogliaro, M. Bearpark, J. J. Heyd, E. N. Brothers, K. N. Kudin, V. N. Staroverov, T. A. Keith, R. Kobayashi, J. Normand, K. Raghavachari, A. P. Rendell, J. C. Burant, S. S. Iyengar, J. Tomasi, M. Cossi, J. M. Millam, M. Klene, C. Adamo, R. Cammi, J. W. Ochterski, R. L. Martin, K. Morokuma, O. Farkas, J. B. Foresman, D. J. Fox, *Gaussian 16*, Revision C.02, Gaussian, Inc., Wallingford CT, 2019.
4. R. Dennington, T. A. Keith, J. M. Millam, *GaussView*, Version 6.0.16, Semichem Inc., Shawnee Mission, KS, **2016**.